Macromolecules **1995,** *28,* 5029−5036 **5029**

Study of the Phase Structure of Linear Polyethylene by Means of Small-Angle X-ray Scattering and Raman Spectroscopy

Norbert Stribeck,[†] Rufina G. Alamo,[‡] Leo Mandelkern,[‡] and Hans Gerhard Zachmann[*,†]

Institut für Technische und Makromolekulare Chemie, University of Hamburg, Bundesstrasse 45, 20146 Hamburg, FRG, and Department of Chemistry and Institute of Molecular Biophysics, Florida State University, Tallahassee, Florida 32306-3015

Received September 19, 1994; Revised Manuscript Received February 24, 1995[⊗]

ABSTRACT: A study of the phase structure of two linear polyethylene fractions has been carried out by Raman spectroscopy and from the analysis of the interface distribution function from the SAXS intensity data. Very good agreement is obtained for the core crystallite thickness, the liquid-like region, and the thickness of the interface from these two independent techniques. Moreover, the X-ray analysis distinguishes isothermally formed crystals from quenched crystals in cases where the Raman technique is not selective.

Introduction

The morphological structure of polymers, particularly the thickness of the crystallite and liquid-like regions and the conformations of the chains in these regions, is a subject of continuous interest. The importance of these structural variables, which characterize lamellar crystals, in determining the physical properties of polymers has been recognized in the past.[1−5] Three widely used experimental techniques to obtain these parameters are X-ray scattering, Raman spectroscopy, and electron microscopy. Because the results obtained with each of these techniques did not always agree, previous works were directed to obtaining reasons for these discrepancies.[6,7] In one of these studies the crystallite thicknesses and their distributions were calculated from the longitudinal acoustic mode (LAM) in Raman spectroscopy and from transmission electron microscopy (TEM). A detailed comparison between both techniques was carried out using linear polyethylene fractions.[7,8] Good quantitative agreement between both techniques is obtained when the thickness distribution is narrow. Such distributions are obtained with intermediate molecular weight specimens crystallized at intermediate crystallization temperatures (125−128 °C), provided that the crystallization is rapid and essentially complete before the sample is cooled. Correction also has to be made for the inclination of the chain axes from the normal to the lamellar basal plane (tilt angle). Bimodal or broad distributions add further complications in the analysis, and agreement in these cases is usually not obtained.[7,8]

In the present work the mean crystallite thickness values and their distributions, obtained by the analysis of the LAMs in Raman spectroscopy, will be compared to corresponding values obtained from a detailed analysis of the interface distribution function calculated from the SAXS data. The thickness of the interfacial region where the ordered chains emanating from the crystals gradually lose their order is also an important parameter that can be measured by analysis of the data obtained from these two techniques. The advantages and limitations of both analyses will be presented in the study of two linear polyethylene fractions.

Theoretical Background

The analysis of the internal modes region of the Raman spectrum of polyethylene (900−1550 cm^{-1})[9−11] allows us to obtain the magnitudes of crystalline (α_c), liquid-like (α_a), and interfacial contents (α_b). Following the method initially developed by Strobl,[9]

$$\alpha_c = \frac{I_{1416}}{I_{1295} \times 0.46} \qquad \alpha_a = \frac{I_{1303}}{I_{1295}} \qquad \alpha_b = 1 - (\alpha_c + \alpha_a) \tag{1}$$

where I_{1416} is the intensity of the CH_2 bending band split by the crystal field, I_{1295} is the total intensity in the twisting region which is independent of crystallinity level and serves as an internal standard, I_{1303} is the intensity of the twisting CH_2 band of the liquid-like material, and 0.46 is a scaling coefficient determined from the fully crystallized polyethylene.[9]

In the low-frequency region of the Raman spectrum (5−60 cm^{-1}), the frequency ν of the LAM for a continuous chain in the absence of interchain coupling, is related to the ordered sequence length L_{CR} by the relation[12]

$$\nu_m = \frac{m}{2cL_{CR}}\sqrt{\frac{E_c}{\varrho}} \tag{2}$$

where m is the mode order (m = 1, 3, 5, ...), c is the speed of light, E_c is Young's elastic modulus in the chain direction, and ϱ is the density of the vibrating sequence. For the lamellar-like crystallite type polymers, which consist of ordered and disordered chain sequences, it can be shown that the observed frequency of the LAM-1 is proportional to the length of the ordered sequence by the following eq 2.[13−15] The ordered sequence length distribution, $f(L)$, is obtained by following the relation given by Snyder and Scherer[16] for the temperature−frequency-corrected spectrum:

$$f(L) \propto [1 - \exp(-hc\Delta\bar{\nu}/kT)]\Delta\bar{\nu}^2 I_\nu^{\text{obs}} \tag{3}$$

h, c, and k are the universal Planck, speed of light, and Boltzmann constants. T is the temperature of the sample, $\Delta\bar{\nu}$ is the frequency shift, and I_ν^{obs} is the intensity of the LAM band at a given $\Delta\nu$. One requirement for the applicability of eq 3 is that the width at half-height of the LAM obtained for the polymer be much greater than the natural bandwidth.[16] From the

---

[*] Corresponding author.

[†] University of Hamburg.

[‡] Florida State University.

[⊗] Abstract published in *Advance ACS Abstracts*, June 1, 1995.

0024-9297/95/2228-5029$09.00/0

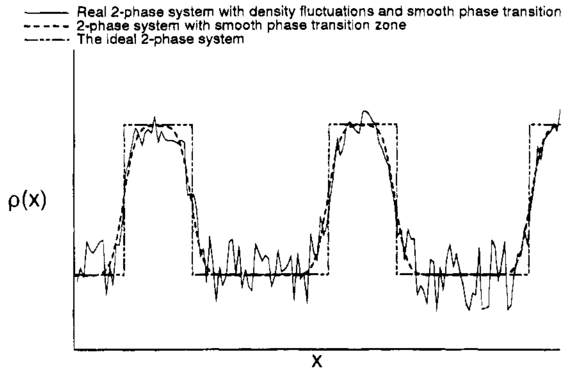

Figure 1. Density profiles of ideal and nonideal two-phase systems, as introduced in SAXS theory.

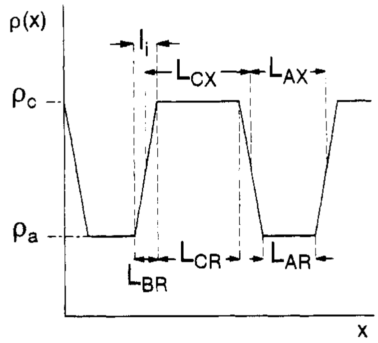

Figure 2. Parameters of a semicrystalline system with diffuse boundaries. Thicknesses determined by SAXS: l_i, $\bar{L}_{CX}$, $\bar{L}_{AX}$. Thicknesses determined by Raman LAM: L_{BR}, L_{CR}, L_{AR}.

shape of the Raman line a distribution of L_{AR} and L_{CR} with the average values $\bar{L}_{AR}$ and $\bar{L}_{CR}$ can be obtained.

From the absolute intensities of the small-angle X-ray scattering (SAXS) data, the one-dimensional correlation function of an isotropic polymer[17-20] or the interface distribution function[21-23] can be computed by following standard methods to evaluate of the distributions.[24-26] From these functions, besides the crystallinity level within lamellar stacks, structural parameters such as the thickness of the crystalline and amorphous regions, as well as that of the transitional boundary, can be obtained. In the present work, although the correlation function is computed, emphasis is given to the determination of the interface distribution function of a system consisting of a crystalline, an amorphous, and an interfacial region. In addition, it is also considered that local electron density fluctuations are present in these regions.

The slit-smeared intensity of the scattering in electron units, as measured by means of a Kratky camera is given by[24,27a]

$$\frac{J(s)}{V} = \frac{r_R}{te^{-\mu t}HL\lambda r_e^{\,2}}\frac{P_R(s)}{P_o} \tag{4}$$

where $P_R(s)$ (in units of counts per second) is the power of the scattered X-ray beam measured by a detector with the slit opening of $H \times L$, r_R is the distance between the sample and the plane of registration, t is the thickness, $e^{-\mu t}$ is the absorption of the sample, λ is the wavelength of the radiation, r_e is Thomson's classical electron radius, and P_o is the primary beam power per unit slit length in the plane of registration; s is the scattering vector with $|\vec{s}| = s = (2 \sin \theta)/\lambda$, θ being half of the scattering angle.

Generally, one has to consider a nonideal semicrystalline system, as indicated in Figure 1, which contains diffuse phase boundaries and statistical fluctuations of the density. A procedure proposed by Ruland and one of us[22,23,26] was used to determine the scattering background caused by statistical fluctuations of the electron density, J_{Fl}, and the thickness, l_i, of the interfacial region between the amorphous and the crystalline layers. This procedure uses a numerical approximation proposed by Koberstein *et al.*[24] to retrieve estimated values of different parameters from a simple plot. According to this approximation the tail of the slit-smeared scattering curve, $J(s)/V$, of a two-phase system containing short range density fluctuations and a finite interfacial region (in this case called a nonideal two-phase system) can be written as

$$\frac{J(s)}{V} \approx \frac{\tilde{A}_P}{s^3}\exp[-38(\sigma s)^{1.81}] + J_{Fl} \tag{5}$$

where σ is the variance of a Gaussian distribution, which generates the smooth phase boundary, and $\tilde{A}_P$ is Porod's asymptote. The width of the transition zone l_i is defined as $l_i = 3\sigma$. In a plot of $\ln[s^3(J(s) - J_{Fl})]$ vs $s^{1.81}$, the value of J_{Fl} is varied until the range in which the data follow a linear decrease is maximized. A straight line is fitted to the data in this linear range, and Porod's asymptote $\tilde{A}_P$ and σ are obtained from the intercept and slope of the straight line, respectively.

After $\tilde{A}_P$, σ, and l_i have been evaluated, the interference function $\tilde{G}_{id}(s)$ of the corresponding ideal two-phase system with no density fluctuations and no interfacial transition zone is calculated from the measured scattering intensity of the nonideal system, $J(s)/V$,[21] by means of the following equation[21]

$$\tilde{G}_{id}(s) = \frac{(J(s)/V - J_{Fl})s^3}{(1 - 8\pi^2\sigma^2 s^2)\operatorname{erfc}(2\pi\sigma s) + 4\sqrt{\pi\sigma s}\exp[-4\pi^2\sigma^2 s^2]} - \tilde{A}_P \tag{6}$$

Following Porod's law, $\tilde{G}_{id}(s)$ should approach zero for large values of s. If this is not the case because of the approximation involved in eq 5, in a second step σ and $\tilde{A}_P$ are varied until this requirement is fulfilled.

As introduced by Ruland,[21] the interface distribution function $g_1(x)$ is obtained by inserting the values of $\tilde{G}_{id}(s)$ calculated from eq 6 into the equation

$$g_1(x) = \frac{\pi}{4}\int_0^\infty \tilde{G}_{id}(s)\left[4J_0(2\pi xs) - 2\left(2\pi xs + \frac{1}{2\pi xs}\right)J_1(2\pi xs)\right] ds \tag{7}$$

Here J_0 and J_1 are Bessel functions of orders zero and one. The evaluation of the thicknesses of the crystalline and the amorphous regions (L_{CX} and L_{AX} in Figure 2) and the long spacing, L, is carried out from the interface distribution function as previously described.[25,26] This figure also shows the thicknesses obtained by Raman spectroscopy, L_{CR}, L_{AR}, and L_{BR}, which will be defined later in the text.

Besides the interface distribution function one can determine the linear correlation function $\gamma_1(x)$ of the ideal two-phase system by means of the equation[16,17]

$$\gamma_1(x) = \frac{2\pi}{Q_{id}}\int_0^\infty \frac{J_{id}(s)}{V}[J_0(2\pi xs) - 2\pi xsJ_1(2\pi xs)]\, ds \tag{8}$$

$J_{id}(s)/V$, the scattering of the ideal two-phase system with sharp transitions between the two phases and a uniform electron density within each phase, can be calculated from $\tilde{G}_{\rm id}(s)$[21] by using the equation

$$\frac{J_{\rm id}(s)}{V} = \left[\frac{\tilde{G}_{\rm id}(s)}{16\pi^2} + \tilde{A}_{\rm P}\right]s^{-3} \qquad (9)$$

From this function the structural parameters which define the phase structure of the system can also be determined,[20,26] if only the two-phase lamellar structure is unimodal and the corresponding layer thickness distributions are not too wide. Both the premises will guarantee that one will be able to find the typical shape at the minimum of the correlation function, which is necessary to start a quantitative analysis of $\gamma_1(x)$.[26]

The invariant, $Q_{\rm id}$, is determined by integrating the smeared SAXS intensity over all scattering angles

$$Q_{\rm id} = 2\pi \int_0^\infty s \frac{J_{\rm id}(s)}{V}\, {\rm d}s \qquad (10)$$

with V as the scattering volume of the sample. $Q_{\rm id}$ is, in addition, related to the structure of an ideal two-phase model,

$$Q_{\rm id} = \phi_{\rm c}(1 - \phi_{\rm c})\Delta\varrho^2 \qquad (11)$$

where $\phi_{\rm c}$ is the volume fraction of the crystals and $\Delta\varrho$ is the density difference between crystals and amorphous regions.

Experimental Section

The two polyethylene fractions used in this work were obtained from the National Bureau of Standards. They are NBS 1484 ($M_{\rm w}$ = 119 600, $M_{\rm w}/M_{\rm n}$ = 1.19) and NBS 1483 ($M_{\rm w}$ = 32 000, $M_{\rm w}/M_{\rm n}$ = 1.11). For the SAXS work, specimens with dimensions of 35 mm × 3 mm × 3 mm were obtained by pressing the original polyethylene powder, contained in a 1 mm thick mold, in a Carver Press at 150 °C. To achieve the required 3 mm thickness, three 1 mm thick specimens were stacked together. The specimens, contained in the mold, were sealed in evacuated glass tubes, melted at 160 °C for 15 min, and rapidly transferred to a silicon oil bath set at the required crystallization temperature controlled with a precision of ±0.1 °C. NBS 1484 was crystallized at 125 °C for 3 h, and NBS 1483, at 127 °C also for 3 h. After the crystallization time was elapsed, the tubes were quenched in ice water. A small piece of these specimens was used for the Raman experiments.

The SAXS measurements were carried out using Ni-filtered Cu Kα radiation, a Kratky compact camera, and a proportional detector with energy discrimination. In order to determine the scattering intensity with the necessary accuracy, the samples were measured using four different entrance slits with vertical dimensions of 30, 50, 80, and 130 μm, respectively, in overlapping angular regions covering a total range of 0.0084 nm^{-1} < s < 0.6 nm^{-1}. The absorption factor and the primary beam power per unit slit length, $P_{\rm o}$, were measured using the moving slit method.[27a] Two-dimensional SAXS patterns were recorded on photographic film using a pinhole camera manufactured by A. Paar.

The Raman spectra were recorded using the incident radiation of 514.5 nm of a coherent INNOVA argon ion laser Model 90 and a SPEX 1403 double monochromator spectrometer equipped with two 2400 lines/mm planar holographic gratings. The plasma lines were removed from the laser beam using a SPEX 1460 Lasermate premonochromator. The value of the Young's modulus for polyethylene was taken as 2.9 × 10^{12} dyn/cm^2.[27b,c]

The melting temperatures were obtained in a Perkin-Elmer DSC 2B differential scanning calorimeter at a heating rate of 10 K/min. Degrees of crystallinity were determined from the area of the endotherms using the heat of fusion of indium (6.8 cal/g) as the reference standard. The heat of fusion was converted to the degree of crystallinity, $(1 - \lambda)_{\Delta H}$, by taking the enthalpy of a pure polyethylene crystal to be 69 cal/g.[28] Densities were measured at room temperature in a triethylene glycol/2-propanol density gradient column calibrated with standard glass floats. Degrees of crystallinity were calculated from the measured densities using the relation given by Chiang and Flory.[29]

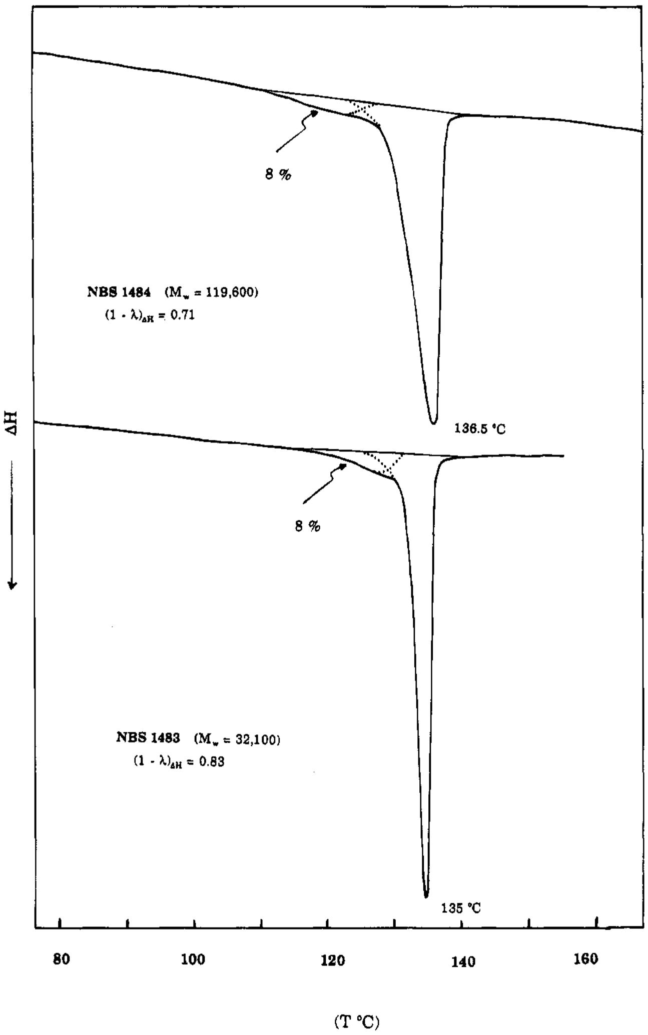

Figure 3. DSC melting thermograms of the two linear PE fractions isothermally crystallized.

Results

An initial characterization of the isothermally crystallized polyethylene fractions was carried out by differential scanning calorimetry. Figure 3 shows the melting peaks of both samples. Both endotherms show a small low-temperature peak, about 8% of the total heat of fusion. This peak corresponds to the fraction of material that crystallizes on cooling. The predominant high-temperature peak is from the crystals formed isothermally.

The volume fraction degree of crystallinity calculated from the density data gave 0.86 ± 0.01 for NBS 1483 and 0.77 ± 0.01 for NBS 1484. These values are slightly higher but similar to those calculated from the heat of fusion (included in Figure 3).

The results from the analyses of the internal mode region (900–1550 cm^{-1}) of the Raman spectra are summarized in Table 1. The core crystallinity levels agree with those calculated from the heat of fusion and are within the range of values expected for isothermally crystallized linear PE fractions.[30] The low interfacial contents (5–7%) found for these samples are also expected for this type of isothermal crystallization.[10] If

Table 1. Results from the Analysis of the Raman Spectra

	α_c [%]	α_a [%]	α_b [%]	$\bar{L}_{CR}$ [Å]	$\bar{L}_{AR}$ [Å]	$\bar{L}_{BR}$ [Å]	$\bar{L}_R$ [Å]
NBS 1484 $T_c = 125$ °C	70	23	7	250	96	12	370
NBS 1483 $T_c = 127$ °C	80	15	5	285	63	8	364

the interfacial content, α_b, is added to the core crystallinity, α_c, the values obtained, 77% and 85%, are almost identical to the crystallinity level calculated from the density. This is in agreement with previous results and reflects the fact that the interphase is included in the measurement of the density but not in the heat of fusion measured by DSC.[10,31]

The crystallite thicknesses calculated from the LAM (L_{CR} in Figure 2) are also included in Table 1. The crystallite thickness is known to increase with crystallization temperature, and accordingly, the NBS 1483 crystals obtained at 127 °C are slightly thicker than those from NBS 1484 which was crystallized at 125 °C. The crystals formed in the quenching process, clearly detected by DSC, are expected to be much thinner, of the order of 100 Å or less. Therefore, the longitudinal acoustic mode from these crystals is expected to appear at much higher frequencies than the LAM from the isothermally formed crystals. However, a second LAM peak was not observed in the low-frequency Raman spectrum. This peak is probably of very low intensity and, assuming that the thin crystals have a broad distribution, the LAM will be broad and most probably buried in the baseline from which the peak will be difficult to extract.

Defining $\bar{L}_{AR}$ as the average thickness of the liquid-like region and $\bar{L}_{BR}$ as the mean thickness of the interphase that is associated with one of the crystallite basal planes (see Figure 2), these quantities can be calculated by assuming a linear three phase model.[32] It follows that the mass crystalline fraction is given by[32-34]

$$\alpha_c = \frac{\bar{L}_{CR}}{(\bar{L}_{AR} + 2\bar{L}_{BR}) + \bar{L}_{CR}} \frac{\varrho_c}{\varrho_T} \tag{12}$$

and the mass interfacial fraction by

$$\alpha_b = \frac{\bar{L}_{BR}}{(\bar{L}_{AR} + 2\bar{L}_{BR}) + \bar{L}_{CR}} \frac{\varrho_b}{\varrho_T} \tag{13}$$

The demoninator $(\bar{L}_{AR} + 2\bar{L}_{BR}) + \bar{L}_{CR}$ represents the long period $\bar{L}_R$, as it is conventionally obtained by small-angle X-ray scattering as well. Note that according to Figure 2 the thickness of the interface region $\bar{L}_{BR}$ has to be added twice when calculating the long period $\bar{L}_R$. α_a, α_b, and α_c are obtained from the Raman spectra according to eq 1 and ϱ_c, ϱ_b, and ϱ_T are the densities of the pure crystalline region, of the interface, and of the sample, respectively. A similar equation will hold for α_a.

The thicknesses of the three regions calculated for the two polyethylene fractions and the long spacing, $\bar{L}_R$, are given in the last four columns of Table 1. In analogy with previous results,[10] the polyethylene with the highest molecular weight shows the highest interfacial thickness. These values are 12 Å for NBS 1484 and 8 Å for NBS 1483 and are very similar to the interfacial thicknesses found for other polyethylene fractions.[10]

As mentioned in the theoretical background, the thicknesses of crystals, of the amorphous regions, and of the interphase can also be calculated from absolute small-angle X-ray scattering data. Figure 4 represents the slit-smeared scattering curves of the two polyethylenes under study. The ordinate represents the absolute scattering intensity per unit volume, integrated along the measuring slit of the Kratky camera (electron units per nm^4), obtained from the power P_R of the scattered radiation by means of eq 4. One can easily see from these curves that sample NBS 1484 shows a higher scattering intensity and a larger long period than sample NBS 1483. This is also seen in the scattering curves represented in Figure 5 obtained after desmearing by using the Guinier–DuMond procedure.[35]

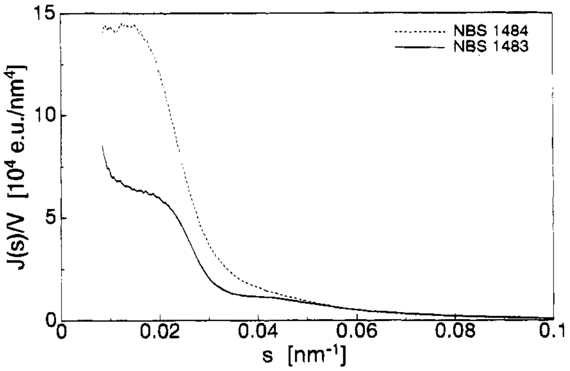

Figure 4. Absolute, slit-smeared SAXS intensity as a function of the magnitude of the scattering vector *s* of the two linear polyethylene samples.

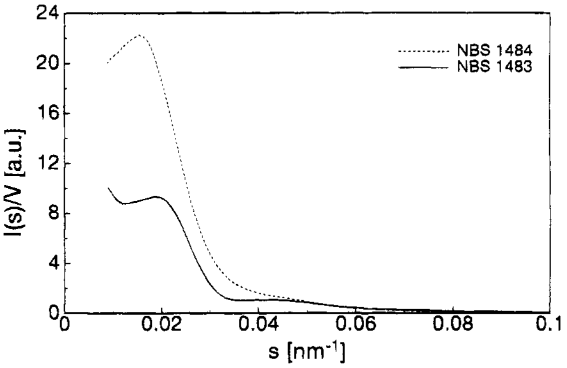

Figure 5. Slit length desmeared SAXS curves of the two polyethylene samples.

From these scattering curves the local electron density fluctuation J_{Fl} which reflects the inhomogeneities within each phase, the average thickness l_i of the interface between the crystals and the amorphous region, and the Porod constant $\tilde{A}_P$ were determined as described in the theoretical section. Equation 5 is plotted in Figure 6 for both samples, and the results are summarized in Table 2. Sample NBS 1483 shows a larger value for the electron density fluctuation J_{Fl} and a somewhat smaller value for the Porod constant $\tilde{A}_P$ than sample NBS 1484. The calculated interfacial values are 18 Å for NBS 1484 and 15 Å for NBS 1483.

In a further evaluation, the scattering of the "corresponding ideal two-phase system" was derived from each of the two scattering curves by subtracting the contribution of J_{Fl} and correcting with respect to the finite value of l_i. Following this, the invariant Q_{id}, the smeared interference function $\tilde{G}_{id}(s)$, the linear correlation function $\gamma_1(x)$, and the interface distribution function $g_1(x)$ of the corresponding ideal two-phase systems were calculated by substitution of $\tilde{A}_P$, l_i, and J_{Fl} of Table 2 in eqs 6–10, respectively.

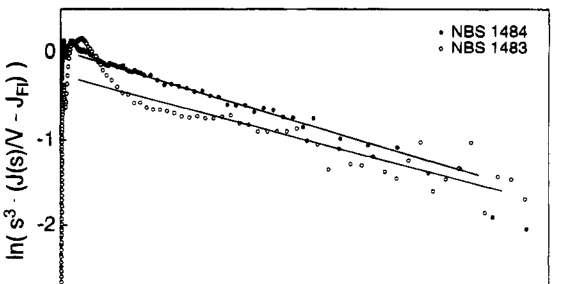

Figure 6. Determination of Porod's law from the measured raw data according to Koberstein et al.[24]

Table 2. Interface Thickness (l_i), Electron Density Fluctuation (J_{Fl}), Porod's Asymptote ($\tilde{A}_P$), and Invariant (Q_{id}) for the Investigated Samples

	l_i [nm]	J_{Fl} [eu/nm^4]	$\tilde{A}_P$[a] [eu/nm^7]	Q_{id}[b] [eu/nm^6]
NBS 1484	1.8 ± 0.2	103 ± 2	0.96 ± 0.13	389 ± 2
NBS 1483	1.5 ± 0.1	147 ± 2	0.60 ± 0.15	317 ± 2

[a] Obtained by means of eq 5. [b] Obtained from eq 10.

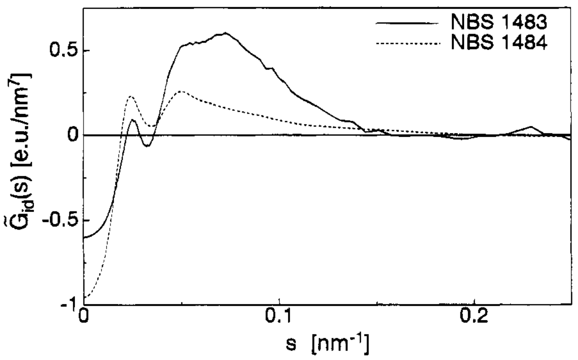

Figure 7. Interference functions $\tilde{G}_{id}(s)$ of the two polyethylene samples.

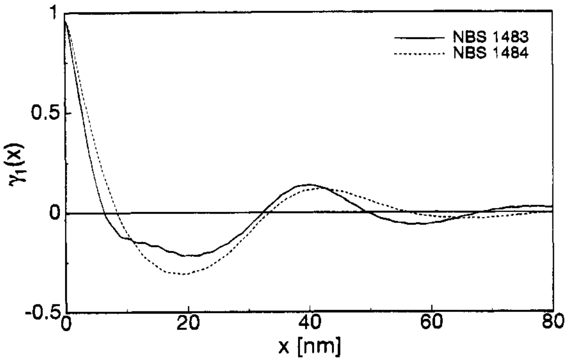

Figure 8. Linear correlation functions $\gamma_1(x)$ of the two polyethylene samples.

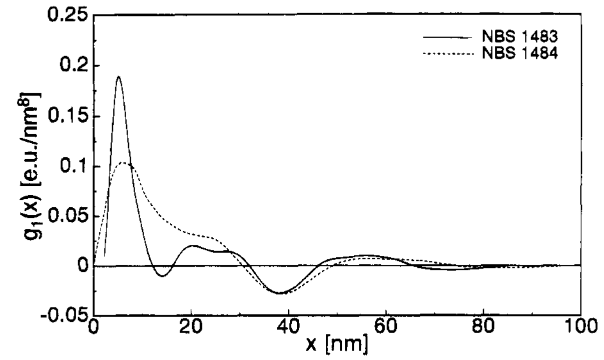

Figure 9. Interface distribution function $g_1(x)$ of the two polyethylene samples.

The values obtained for the invariant are shown in Table 2. The smeared interference functions $\tilde{G}_{id}(s)$ of the two samples are given in Figure 7. One can see that a constant value of $\tilde{G}_{id}(s)$ equal to zero is obtained for s larger than 0.15–0.18 nm^{-1} in agreement with Porod's law. The functions $\gamma_1(x)$ and $g_1(x)$ are represented in Figures 8 and 9. Broad extremes in the curves indicate broad distributions for the values of the long period L_X, the crystal thickness L_{CX}, and the thickness of the amorphous regions L_{AX} in both samples. In addition, a bimodal distribution of those values is indicated in the case of the sample NBS 1483 by both the correlation function (inflection between 12 and 21 nm) and the interface distribution function (minima at 13 and at 39 nm). There is also a suggestion of a bimodal distribution for NBS 1484 from the interface distribution function of Figure 9.

Because the samples present broad distributions, from the SAXS data it is not meaningful to derive average values for L, L_{AX}, and L_{CX} from the positions of the maximum and minima of the interface distribution function or from the corresponding points in the correlation function. Instead, the distributions were determined by assuming a model and fitting the parameters of the model to the measured scattering curves. Two different cases were computed by assuming Gaussian distribution functions for L_{CX} and L_{AX}. In one instance a unimodal distribution of the thicknesses of the two phases was considered and in a second case a bimodal distribution was treated. The probabilities for a value L_{CX} and for a value L_{AX} are then given by

$$w(L_{CX}) = \frac{1}{\sqrt{2\pi}\sigma_C} \exp\left[-\frac{(L_{CX} - \bar{L}_{CX})^2}{2{\sigma_C}^2}\right] \qquad (14)$$

and

$$w(L_{AX}) = \frac{1}{\sqrt{2\pi}\sigma_A} \exp\left[-\frac{(L_{AX} - \bar{L}_{AX})^2}{2{\sigma_A}^2}\right] \qquad (15)$$

respectively. $\bar{L}_{CX}$ and $\bar{L}_{AX}$ are the mean values of L_{CX} and L_{AX}, respectively, and σ_C and σ_A are the standard deviations of the distributions. The mean value of the long period, $\bar{L}_X$, is given by

$$\bar{L}_X = \bar{L}_{CX} + \bar{L}_{AX} \qquad (16)$$

In the same way, the mean values of the distances of the other interfaces were calculated. The standard deviations are parameters which could be varied.

When bimodal distributions are assumed, L_{CX} and L_{AX} are characterized by nine adjustable parameters: $\bar{L}_{CX}^{(1)}$, $\bar{L}_{CX}^{(2)}$, $\bar{L}_{AX}^{(1)}$, $\bar{L}_{AX}^{(2)}$, $\sigma_C^{(1)}$, $\sigma_C^{(2)}$, $\sigma_A^{(1)}$, $\sigma_A^{(2)}$, and the volume fraction $\Phi^{(1)}$ of component 1.

The parameters $\bar{L}_{CX}$ and $\bar{L}_{AX}$ and the standard deviations in the case of the unimodal distribution, and $\bar{L}_{CX}^{(1)}$, $\bar{L}_{CX}^{(2)}$, $\bar{L}_{AX}^{(1)}$, $\bar{L}_{AX}^{(2)}$, and the standard deviations in the case of the bimodal distributions, were varied until a best fit between the calculated and measured scattering curves was obtained. The values of the parameters which give the best fit are listed in Table 3 for the unimodal distribution and in Table 4 for the bimodal distribution, respectively. The interface distribution functions calculated by using these values are plotted together with the corresponding measured functions in Figures 10 and 11. Both unimodal and bimodal distri-

Table 3. Best Fit Results for the Average Thickness of the Crystals ($\bar{L}_{CX}$) and of the Amorphous Regions ($\bar{L}_{AX}$), the Long Period ($\bar{L}_X$), the Standard Deviations (σ_C, σ_A, σ_L), and the Volume Fraction of Crystals within the Lamellar Stacks (Φ_{CL}) Obtained by Assuming Unimodal Distribution[a]

	NBS 1484	NBS 1483
$\bar{L}_{CX}$ [nm]	22.1 ± 0.1	26.6 ± 0.3
$\sigma_C/\bar{L}_{CX}$	0.36 ± 0.01	0.24 ± 0.01
$\bar{L}_{AX}$ [nm]	6.7 ± 0.1	5.4 ± 0.1
$\sigma_A/\bar{L}_{AX}$	0.70 ± 0.02	0.40 ± 0.01
$\bar{L}_X$ [nm]	28.9 ± 0.2	0.40 ± 0.01
$\sigma_L/\bar{L}_X$	0.69 ± 0.04	0.33 ± 0.02
Φ_{CL}	0.768 ± 0.003	0.831 ± 0.003

[a] The errors are only the estimated errors of the fit.

Table 4. Best Fit Results for the Average Thickness of the Crystallites ($\bar{L}_{CX}^{(1)}$, $\bar{L}_{CX}^{(2)}$) and of the Amorphous Regions ($\bar{L}_{AX}^{(1)}$, $\bar{L}_{AX}^{(2)}$), the Average Long Periods ($\bar{L}_X^{(1)}$, $\bar{L}_X^{(2)}$), the Standard Deviation of These Quantities ($\sigma_C^{(1)}$, $\sigma_C^{(2)}$, $\sigma_A^{(1)}$, $\sigma_A^{(2)}$, $\sigma_L^{(1)}$, $\sigma_L^{(2)}$), the Volume Fractions of the Crystals within the Lamellar Stacks ($\Phi_{CL}^{(1)}$, $\Phi_{CL}^{(2)}$), and the Volume Fraction of the Major Component ($\Phi^{(1)}$) Obtained by Assuming Bimodal Distributions[a]

	NBS 1484	NBS 1483
$\bar{L}_{CX}^{(1)}$ [nm]	28.4 ± 0.2	29.3 ± 0.3
$\sigma_C^{(1)}/\bar{L}_{CX}^{(1)}$	0.28 ± 0.02	0.21 ± 0.02
$\bar{L}_{AX}^{(1)}$ [nm]	9.2 ± 0.2	5.5 ± 0.1
$\sigma_A^{(1)}/\bar{L}_{AX}^{(1)}$	0.60 ± 0.01	0.41 ± 0.02
$\bar{L}_X^{(1)}$ [nm]	37.6 ± 0.3	34.8 ± 0.4
$\sigma_L^{(1)}/\bar{L}_X^{(1)}$	0.30 ± 0.02	0.24 ± 0.01
$\Phi_{CL}^{(1)}$	0.756 ± 0.008	0.843 ± 0.003
$\Phi^{(1)}$	0.80 ± 0.02	0.95 ± 0.03
$\bar{L}_{CX}^{(2)}$ [nm]	7.3 ± 0.1	5.1 ± 0.2
$\sigma_C^{(2)}/\bar{L}_{CX}^{(2)}$	0.30 ± 0.01	0.19 ± 0.03
$\bar{L}_{AX}^{(2)}$ [nm]	3.8 ± 0.1	6.7 ± 0.2
$\sigma_A^{(2)}/\bar{L}_{AX}^{(2)}$	0.48 ± 0.03	?
$\bar{L}_X^{(2)}$ [nm]	11.1 ± 0.2	11.8 ± 0.2
$\sigma_L^{(2)}/\bar{L}_X^{(2)}$	0.9 ± 0.2	0.38 ± 0.02
$\Phi_{CL}^{(2)}$	0.66 ± 0.07	0.43 ± 0.02

[a] The errors are only the estimated errors of the fit.

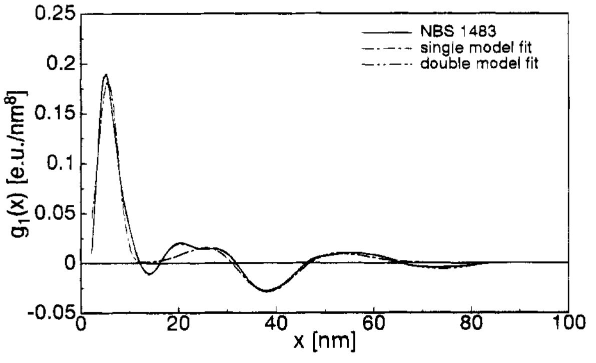

Figure 10. Interface distribution function $g_1(x)$ of NBS 1483 and fitted curves.

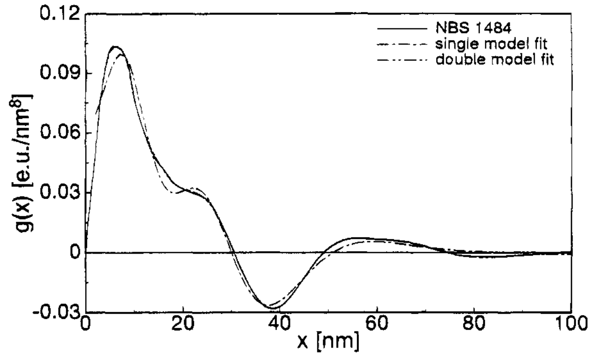

Figure 11. Interface distribution function $g_1(x)$ of NBS 1484 and fitted curves.

butions give reasonable fits. However, a better agreement is found between the measured and the calculated curves when the bimodal distribution is used. Table 4 shows that the minor component of the bimodal distribution of sample NBS 1483 is only about 5%. For sample NBS 1484 the magnitude of the minor component that fits the measured scattering curve is much higher, about 20%, which makes a considerable contribution to the scattering.

The volume fraction of crystals within the lamellar stacks, Φ_{CL}, calculated from the $\bar{L}_{CX}$ and $\bar{L}_X$ values used in the unimodal or bimodal fit (major component) agrees closely with the crystallinity values calculated from the measured densities for both samples. This indicates that stacked lamellae are filling the majority of the volume sample and that the volume fraction of crystals within the lamellar stacks of the calculated 20% minor component in NBS 1484 is also relatively high compared to that of the major component.

Discussion

Validity of the Linear Model. For the data evaluation of both Raman and SAXS measurements a linear model was assumed. This included that all the amorphous phase is located in the layers between the lamellar crystals and no amorphous material is lateral to the lamellar stacks. The validity of the assumption can be tested by comparing the linear crystallinity obtained by SAXS and Raman with the crystallinity measured by DSC and/or density. As is shown in the Results, they are not significantly smaller than the values obtained by SAXS and Raman. Therefore the assumption of a linear model appears to be allowed.

Interfacial Thickness. The data characterizing the morphology of polyethylene fractions, obtained by Raman spectroscopy (Table 1) and SAXS (Tables 3 and 4), can now be compared and discussed.

Of relevant interest are the thicknesses of the crystalline, liquid-like, and interfacial regions obtained by both techniques. These data are compiled in Table 5. The interfacial thicknesses obtained by Raman spectroscopy (L_{BR}) are 12 Å for the fraction of highest molecular weight which was crystallized at 125 °C and 8 Å for the NBS 1483 crystallized at a slightly higher temperature. It was previously found[10,32] that decreasing molecular weight and/or increasing crystallization temperature results in crystallites of lower interfacial content and lower interfacial thicknesses. The interfacial thicknesses calculated from the SAXS data, $l_i = \bar{L}_{BX}$, (Figure 6) are 18 and 15 Å for the high and low molecular weight fractions, respectively. These values are not only of the same order of magnitude but also very similar to those obtained from the Raman method. It is worth noting that the interfacial thicknesses obtained from SAXS, as calculated from eq 5, are generated before computing the interface distribution function.

The importance of obtaining similar interfacial thicknesses from two different, independent techniques, that are also in agreement with those obtained by other methods (see ref 36 and references herein), is obvious. It confirms the validity of using these techniques to quantify the phase structure of semicrystalline polymers. The results obtained with the two fractions analyzed confirm the adequacy of the three-phase model used to analyze the phase structure from the Raman

Table 5. Comparison of Raman LAM Results with SAXS Results

	$\bar{L}_{BR}$ [Å]	$\bar{L}_{BX} = l_i$ [Å]	$\bar{L}_{CR}$ [Å]	$\bar{L}_{CX} - \bar{L}_{BX}$ [Å]	$\bar{L}_{AR}$ [Å]	$\bar{L}_{AX} - \bar{L}_{BX}$ [Å]	$\bar{L}_R$ [Å]	$\bar{L}_X$ [Å]
NBS 1484 $T_c = 125$ °C	12 ± 4	18 ± 2	250 ± 10	266 ± 10	96 ± 4	74 ± 10	370	376
NBS 1483 $T_c = 127$ °C	8 ± 4	15 ± 1	285 ± 10	278 ± 10	63 ± 4	40 ± 10	364	348

spectroscopy data. The similarity between the $\bar{L}_{BR}$ and $\bar{L}_{BX}$ values also indicate that the assumption made in the development of eq 5 are adequate in the study of these types of samples.

Bimodal Distribution Function. It was found in this study that the interface distribution function computed from the absolute X-ray data, was better fitted by bimodal distributions than by only taking a single average thickness component. Although the calculated curves require the assumption of nine adjustable parameters to calculate the bimodal distribution function, the use of this model is justified for its agreement with the results from DSC. The DSC thermograms indicated that about 8% of the transformation takes place in the form of thin crystals formed after quenching. The percentages of the minor component of the bimodal fit are 5% for NBS 1483 (crystallized at the highest temperature) and 20% for NBS 1484. The 5% percentage agrees well with the magnitude of quenched crystals observed in DSC. The percentage used in the bimodal fit for NBS 1484 is high compared to the DSC value; however, taking into account the experimental errors in both determinations, these numbers are not unreasonable. Perhaps absolute measurements of heat capacities and/or the use of different mathematical functions to model layer thickness distributions and electron density fluctuations will make these percentages closer.

An important implication in this analysis is that the X-ray data are informative about the double population of crystallites in these samples whereas the Raman LAM technique did not distinguish the crystallites formed on quenching.

A bimodal distribution of thicknesses for the sample NBS 1483 is already indicated in Figure 7. The existence of two kinds of stacks is also clear in the correlation curve of Figure 8 by the comparatively broad minimum which can be decomposed into two superposing minima. In addition, it is clearly manifested in the interface distribution function by the appearance of two minima at 13 and 39 nm corresponding to two values of the long period. The first minimum is interpreted as a long period because it is followed by two maxima (at 19 and 23 nm). The minimum at 39 nm cannot be interpreted as the second order of the one at 13 nm since the average value of L determined from the scattering curve is close to 39 nm and not to 13 nm and also because 39 nm is not twice 13 nm. The assumption of two different distributions is, therefore, justified with the finding of two different long periods.

The presence of a second long period for the sample NBS 1484 from the correlation function or the interface distribution curve (Figures 8 and 9) is not as clear as in NBS 1483. However, the agreement between calculated and measured curves is not as good if only one component is assumed (see Figure 11).

In a previous study on PET[37] the assumption of asymmetric unimodal distributions led to a considerable improvement of the single component fit. However in the present study with polyethylene fractions the fit is not improved when the symmetrical Gaussian thickness distributions are replaced by skewed Gaussian distributions in the model function. On the other hand, if one considers asymmetric layer thickness distributions, there is a choice from numerous functions, some of which may be more appropriate to describe stacks from layers with rather smooth surfaces than skewed Gaussian distributions.[38]

The authors are aware of the fact that, for the sake of simplicity, one would prefer a one model fit. Therefore, both evaluations have been performed and it is left up to the reader which fit he prefers. Nevertheless, the authors want to stress that because of reasons discussed above they strongly believe that the two model fit, at least in the case of sample NBS 1483, is well supported by the results.

Phase Structure and Crystallite Thickness Distribution. Before a comparison of the core crystallite thickness, the liquid-like region, and the long period between the data obtained from Raman and those from SAXS could be done, it needs to be pointed out that the crystallite thickness obtained from X-rays does not correspond to that calculated from the Raman LAM. The differences can be seen clearly in the electron density profile of Figure 2. Because $\bar{L}_{CX}$ and $\bar{L}_{AX}$ are computed using an equation formulated for a two-phase ideal system, the value of l_i (interface) needs to be subtracted from $\bar{L}_{CX}$ and $\bar{L}_{AX}$ in order to make these variables comparable to the Raman values. The corrected values are listed in Table 5. In this table, C and A stand for crystalline and amorphous regions and R and X for the Raman or X-ray data, respectively. Only the X-ray data for the major component are considered for comparison in Table 5.

In spite of the different methods of experimentation, the values of the core crystallite thickness are remarkably similar for both fractions analyzed. Similar values are also obtained for the thickness of the liquid-like region as well as for the long period ($\bar{L}X$, $\bar{L}_R$). The agreement between these two independent techniques is excellent and supports their use in studying the phase structure of the polyethylenes.

A possible tilt of the chains in the crystal was not considered in the calculations of $\bar{L}_{CR}$, $\bar{L}_{BR}$, and $\bar{L}_{AR}$ listed in Tables 1 and 5. If a 20° tilt is considered, the value of $\bar{L}_{CR}$ decreases by about 15 Å, but the thicknesses are still very similar to those found by the X-ray technique.

The crystallite thickness distributions were also computed from the Raman LAM data, by following eq 2 and from the parameters resulting from the fit to the SAXS data, using eq 14.

The distributions are compared in Figure 12 for the lowest molecular weight fraction and in Figure 13 for NBS 1484. For both fractions the most probable value of the major component of the bimodal distribution calculated according to SAXS data analysis agrees with the Raman-calculated curves. The width of the distribution calculated from the SAXS technique is, howeve, larger than that calculated from Raman. For the low molecular weight sample the difference in width at half-height of the thickness distribution from both techniques is within the experimental error of the measurement. For the NBS 1484 fraction the half-width of the SAXS distribution is higher than the one from the LAM. The theoretical treatment used to deconvolute the

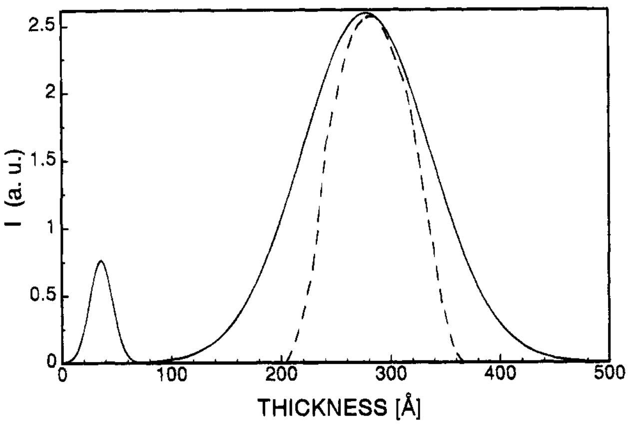

Figure 12. Crystallite thickness distribution of NBS 1483 crystallized at 127 °C: (—) obtained from SAXS; (- - -) obtained from Raman LAM.

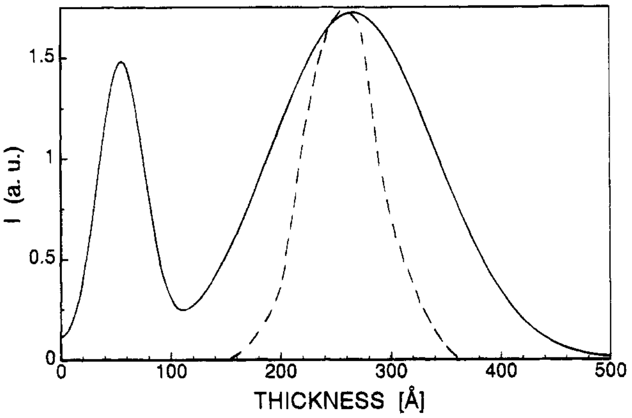

Figure 13. Crystallite thickness distribution of NBS 1484 crystallized at 125 °C: (—) obtained from SAXS; (- - -) obtained from Raman LAM.

components of the phase structure from the interface distribution function, for example the use of theoretical Gaussian distributions in the examples treated in this work, leads to broader distributions than those obtained from more direct methods like those from the LAM peaks. It seems that the use of more complex mathematical approaches should alleviate these differences. The choice of other theoretical functions is, of course, conditioned to knowing the distribution by an additional experimental technique.

Volume Crystallinity and the Linear Model. For the data evaluation of both Raman and SAXS measurements a one-dimensional model was assumed. This means that the layer stacks are assumed to be infinitely extended in both longitudinal and lateral directions. Thus one has to bear in mind that these linear crystallinities may be higher than the true volume crystallinities, if the sample contains amorphous material outside the stacks. As expected, the volume crystallinities determined from Raman ($\alpha_c + \alpha_b/2$) and SAXS ($\Phi_{CL}^{(1)}\Phi^{(1)} + \Phi_{CL}^{(2)}(1 - \Phi^{(1)})$) are identical. For the present samples we have additionally determined the volume crystallinity from density measurements and by DSC. Only if these volume crystallinities were significantly lower than the values determined by the SAXS and the Raman method should one consider the presence of amorphous material outside the lamellar stacks. This is only the case for the DSC method and the sample NBS 1484, where the DSC volume crystallinity (68%) is 6% lower than the value from Raman spectroscopy and SAXS. For the sample NBS 1483 the DSC gives the same volume crystallinity as Raman and SAXS. Crystallinity from density gives values which are even 3% higher than the values from the Raman and SAXS methods. Hence the results from DSC and density do not support the notion of amorphous material outside the stacks.

Acknowledgment. Support of the work at Florida State University by the National Science Foundation Polymer Program Grant DMR 86-13007 is gratefully acknowledged.

References and Notes

(1) Magill, J. H. In *Treatise on Materials Science and Technology*; Schultz, J. M., Ed.; Academic Press: New York, 1977.
(2) Mandelkern, L. *Acc. Chem. Res.* **1976**, *9*, 81.
(3) Mandelkern, L. *J. Polym. Sci., Polym. Symp.* **1975**, *50*, 457.
(4) Keller, A. *Macromolecular Science*; Butterworths: London, 1972; Vol. 8, p 105.
(5) Mandelkern, L. *Polym. J.* **1985**, *17*, 337.
(6) Voigt-Martin, I. G.; Mandelkern, L. *J. Polym. Sci., Polym. Phys. Ed.* **1984**, *22*, 1901.
(7) Voigt-Martin, I. G.; Stack, G. M.; Peacock, A. J.; Mandelkern, L. *J. Polym. Sci., Polym. Phys. Ed.* **1989**, *27*, 957.
(8) Voigt-Martin, I. G.; Mandelkern, L. *J. Polym. Sci., Polym. Phys. Ed.* **1989**, *27*, 987.
(9) Strobl, G. R.; Hagedorn, W. J. K. *J. Polym. Sci., Polym. Phys. Ed.* **1978**, *16*, 1181.
(10) Glotin, M.; Mandelkern, L. *Colloid Polym. Sci.* **1982**, *260*, 182.
(11) Mandelkern, L.; Peacock, A. J. *Polym. Bull.* **1986**, *16*, 529.
(12) Mizushima, S. I.; Shimanouchi, T. J. *J. Am. Chem. Soc.* **1949**, *71*, 1320.
(13) Peticolas, W. L.; Hibler, G. W.; Lippert, J. L.; Peterlin, A.; Olf, H. G. *Appl. Phys. Lett.* **1971**, *18*, 87.
(14) Snyder, R. G. In *Methods of Experimental Physics*; Fava, R. A., Ed.; Academic Press: New York, 1980; Vol. 16, Part A, p 73.
(15) Rabolt, J. F. *CRC Crit. Rev. Solid State Mater. Sci.* **1985**, *12*, 165.
(16) Snyder, R. G.; Krause, S. J.; Scherer, J. R. *J. Polym. Sci., Polym. Phys. Ed.* **1978**, *16*, 1593.
(17) Vonk, C. G.; Kortleve, G. *Kolloid-Z.* **1967**, *220*, 19.
(18) Vonk, C. G.; Kortleve, G. *Kolloid-Z.* **1968**, *221*, 124.
(19) Vonk, C. G. *J. Appl. Crystallogr.* **1973**, *6*, 81.
(20) Strobl, G. R.; Schneider, M. *J. Polym. Sci., Polym. Phys. Ed.* **1980**, *18*, 1343.
(21) Ruland, W. *Colloid Polym. Sci.* **1977**, *255*, 417.
(22) Stribeck, N.; Ruland, W. *J. Appl. Crystallogr.* **1978**, *11*, 535.
(23) Stribeck, N. Dissertation Marburg, 1980.
(24) Koberstein, J. T.; Morra, B.; Stein, R. S. *J. Appl. Crystallogr.* **1980**, *13*, 34.
(25) Polizzi, S.; Stribeck, N.; Zachmann, H. G.; Bordeianu, R. *Colloid Polym. Sci.* **1989**, *267*, 281.
(26) Santa Cruz, C.; Stribeck, N.; Zachmann, H. G.; Balta Calleja, F. J. *Macromolecules* **1991**, *24*, 5980.
(27) (a) Stabinger, H.; Kratky, O. *Makromol. Chem.* **1978**, *179*, 1655. (b) Strobl, G. R.; Eckel, R. *J. Polym. Sci., Polym. Phys. Ed.* **1976**, *14*, 913. (c) Snyder, R. G.; Strauss, H. L.; Alamo, R. G.; Mandelkern, L. *J. Chem. Phys.* **1994**, *100*, 5422.
(28) Flory, P. J.; Vrij, A. J. *J. Am. Chem. Soc.* **1963**, *85*, 3548.
(29) Chiang, R.; Flory, P. J. *J. Am. Chem. Soc.* **1961**, *83*, 2057.
(30) Ergoz, E.; Fatou, J. G.; Mandelkern, L. *Macromolecules* **1972**, *5*, 147.
(31) Mandelkern, L. In *Polymer Characterization*; Craver, C. D., Provder, T., Eds.; Advances in Chemistry Series Vol. 227; American Chemical Society: Washington, DC, 1990; p 377.
(32) Mandelkern, L.; Alamo, R. G.; Kennedy, M. A. *Macromolecules* **1990**, *23*, 4721.
(33) Alamo, R. G.; Viers, B. D.; Mandelkern, L. *Macromolecules* **1993**, *26*, 5740.
(34) Alamo, R. G.; Mandelkern, L. *Thermochim. Acta* **1994**, *238*, 155.
(35) DuMond, J. W. M. *Phys. Rev.* **1947**, *72*, 83.
(36) Mandelkern, L. *Chemtracts: Macromol. Chem.* **1992**, *3*, 347.
(37) Stribeck, N. *Colloid Polym. Sci.* **1993**, *271*, 1007.
(38) Stribeck, N. *J. Phys. IV C8*, **1993**, *3*, 507.

MA946288S